



Original Article

Spatially varying phytoplankton seasonality on the Northwest Atlantic Shelf: a model-based assessment of patterns, drivers, and implications

Zhengchen Zang ^{1,*}, Rubao Ji ¹, Zhixuan Feng ², Changsheng Chen³, Siqi Li³, and Cabell S. Davis¹

¹Department of Biology, Woods Hole Oceanographic Institution, Woods Hole, MA 02543-1050, USA

²State Key Laboratory of Estuarine and Coastal Research, School of Marine Sciences, East China Normal University, Shanghai 200062, China

³School for Marine Science and Technology, University of Massachusetts Dartmouth, New Bedford, MA 02747, USA

*Corresponding author: tel: +225-421-4719; e-mail: zzang@whoi.edu

Zang, Z., Ji, R., Feng, Z., Chen, C., Li, S., Davis, C. S. Spatially varying phytoplankton seasonality on the Northwest Atlantic Shelf: a model-based assessment of patterns, drivers, and implications. – ICES Journal of Marine Science, 78: 1920–1934.

Received 18 October 2020; revised 30 April 2021; accepted 6 May 2021; advance access publication 3 June 2021.

The signal of phytoplankton responses to climate-related forcing can be obscured by the heterogeneity of shelf seascapes, making them difficult to detect from fragmented observations. In this study, a physical–biological model was applied to the Northwest Atlantic Shelf to capture the seasonality of phytoplankton. The difference in phytoplankton seasonality between the Mid-Atlantic Bight (MAB) and the Gulf of Maine (GoM) is a result of the interplay between nutrients and temperature: In the MAB, relatively high temperature in the cold season and longer oligotrophic environment in the warm season contribute to an earlier winter bloom and a later fall bloom; in the GoM, low temperature and strong mixing limit phytoplankton growth from late fall to early spring, resulting in a later spring bloom and an earlier fall bloom. Although the temperature difference between the GoM and the MAB might decrease in the future, stratification and surface nutrient regimes in these two regions will remain different owing to distinct thermohaline structures and deep-water intrusion. The spatial heterogeneity of phytoplankton dynamics affects pelagic and benthic production through connections with zooplankton and benthic–pelagic coupling.

Keywords: Gulf of Maine, marine ecosystem modeling, Mid-Atlantic Bight, phytoplankton seasonality, spatial heterogeneity, thermal sensitivity

Introduction

The Northwest Atlantic Shelf (NAS) from the Gulf of Maine (GoM) to the Mid-Atlantic Bight (MAB) has long been recognized as a highly productive ecosystem, providing essential habitat for breeding, spawning, and feeding of abundant marine life (Mills *et al.*, 2013; Goode *et al.*, 2019). As the foundation of the pelagic food web, phytoplankton supports the marine ecosystem by converting inorganic carbon and nutrients to organic compounds. On the NAS, the seasonality of phytoplankton dynamics plays an important role in nutrient cycling and the phenology of higher trophic levels (Staudinger *et al.*, 2019). Therefore, a comprehensive understanding of phytoplankton dynamics at the seasonal time scale and

its spatial heterogeneity is essential for detecting the impacts of climate-forced ecosystem changes and supporting ecosystem-based fisheries management.

Nitrogen is a predominant limiting nutrient for phytoplankton growth in the NAS ecosystem, and its seasonal variation in the euphotic layer is modulated by stratification and mixing (O'Reilly and Busch, 1984; Townsend *et al.*, 2006). New nitrogen over the NAS is provided by terrestrial discharge, atmospheric deposition, and inflow from the open ocean (Townsend *et al.*, 2010; Zhang *et al.*, 2013; Friedrichs *et al.*, 2019). In the GoM, the intrusion of slope water through the Northeast Channel acts as a major source of dissolved inorganic nitrogen (Ramp *et al.*, 1985; Townsend *et al.*, 2010). After entering the GoM, nutrient-rich deep waters are brought to

the surface via multiple physical processes (e.g. tidal mixing, upwelling, and convective overturning). Fluvial discharge is another source of new nitrogen in the GoM nearshore areas with limited offshore expansion (Townsend *et al.*, 2010). Compared with new nitrogen from external reservoirs, internally recycled nitrogen in the GoM has gained more attention recently, with both model results and field measurements suggesting its importance in supporting surface productivity (Townsend, 1998; Switzer *et al.*, 2020). In the MAB, the impact of terrestrial nutrient fluxes is also largely limited to nearshore areas, although the contribution of nutrient load from large estuarine systems is higher than that in the GoM (Fennel *et al.*, 2006; Zhang *et al.*, 2019). Over the shelf break, cross-frontal mixing events between slope and shelf waters provide additional nitrogen flux into the MAB (Malone *et al.*, 1983; Townsend *et al.*, 2006; Friedrichs *et al.*, 2019).

Phytoplankton dynamics over the NAS are characterized by pronounced seasonality and spatial heterogeneity. In the GoM, phytoplankton have a major bloom in winter–spring and a secondary bloom in fall (Thomas *et al.*, 2003). Lower chlorophyll concentration in summer is due to surface nutrient depletion associated with strong vertical stratification (Tian *et al.*, 2014; Li *et al.*, 2015). Both observations and model results indicate that surface freshening due to Scotian Shelf Water inflow has likely enhanced vertical stratification and contributed to an earlier spring bloom with reduced magnitude in the GoM (Ji *et al.*, 2007, 2008b; Song *et al.*, 2010). In fall, nutrient replenishment from weakened stratification fuels the secondary bloom, and the interannual variability of its formation is related to vertical mixing and pre-bloom conditions (Hu *et al.*, 2011). In the MAB, the seasonal variation of phytoplankton is out of phase with that in the GoM: the winter bloom on the inner shelf of the MAB occurs prior to the spring bloom in the GoM (Yoder *et al.*, 2001; Xu *et al.*, 2011). The timing and magnitude of phytoplankton biomass accumulation in the MAB are largely controlled by water stratification (Xu *et al.*, 2011).

The size structure of phytoplankton communities can affect the efficiency and fate of primary production, and its seasonality can be influenced by physical–biogeochemical conditions on the shelf, including vertical mixing, wind, light, temperature, and nutrient availability (Mouw and Yoder, 2005, 2010). Overall, the eutrophic environment favours a high abundance of large phytoplankton (e.g. diatom). In the GoM, both field measurements and satellite data indicate that mixing-induced strong nutrient replenishment in winter results in the dominance of diatoms during winter–spring, and community cell size decreases from nearshore area to deep basins as the nutrient availability reduces seaward (Mouw and Yoder, 2005; Townsend *et al.*, 2010; Pan *et al.*, 2011). During the summer season, small phytoplankton (e.g. nanophytoplankton) are dominant due to strong vertical stratification and surface nutrient depletion (Li *et al.*, 2006). In the MAB, the seasonality of phytoplankton size structure is controlled by the similar mechanism as that in the GoM (Pan *et al.*, 2011). Most of the previous studies focused on the GoM and the MAB separately, and a model-based integrative framework is needed to synthesize the spatiotemporal patterns and to better understand the driving mechanisms.

Over the NAS, another understudied problem is the dynamics of organic detritus and phytoplankton at the bottom and their coupling with surface productivity. Bottom detritus and phytoplankton are critical energy sources for benthic organisms, including some important fishery species (Townsend and Cammen, 1988; Mills *et al.*, 2013). The abundance of detritus and phytoplankton at the bottom are jointly modulated by vertical sinking from the overlying

water column, lateral advection, and resuspension (Cranford and Gordon, 1992; Dunne *et al.*, 2005). These physical processes, together with biogeochemical dynamics (e.g. particulate organic matter decomposition), regulate the spatial distribution of phytoplankton and detritus at the bottom and the energy flow from the euphotic zone to the benthos. A model-based analysis can shed light on the general spatiotemporal patterns of pelagic–benthic coupling and identify the key gaps in our observations.

Our understanding of nutrient cycling and physical–biological coupling on the NAS has greatly improved over the last few decades (e.g. Malone *et al.*, 1983; Fennel *et al.*, 2006; Ji *et al.*, 2008a, 2008b; Townsend *et al.*, 2014; Zhang *et al.*, 2019). Yet some key questions regarding the spatial heterogeneity of nutrient–phytoplankton dynamics in this ecosystem remain and can be better addressed within an integrative modelling framework. Those questions include (1) What is the major difference between the GoM and the MAB with regard to the seasonality of phytoplankton community? (2) What are the key factors controlling the spatial heterogeneity of phytoplankton dynamics? (3) What are the region-specific responses of phytoplankton dynamics to climate forcing on the NAS? and (4) what are the implications of spatially heterogeneous phytoplankton dynamics for regional pelagic and benthic production. Answering these questions becomes imperative as the climate warming on the NAS seems to be accelerating (Belkin, 2009; Burrows *et al.*, 2011). The objective of this study is to establish a modelling framework to synthesize observational data from various sources, and to identify the major patterns and responsible drivers of the spatially variable phytoplankton seasonality. The 3D coupled physical–biological model used in this study is capable of (1) resolving latitudinal gradients and coastal–shelf–slope interactions; (2) assessing sub-seasonal to interannual variabilities; and (3) resolving pelagic microbial food web dynamics and size-dependent functional responses to changing environmental conditions. Our study focuses on the climatological patterns of nutrient and phytoplankton seasonality based on a multiyear (1978–2014) model simulation described below. Analyses of interannual variability will be presented in follow-up papers.

Material and methods

Ocean hydrodynamic model

The ocean hydrodynamic model used to force the biological model is a three-dimensional, unstructured grid, and primitive equation Finite Volume Community Ocean Model (FVCOM; Chen *et al.*, 2003). Specifically, FVCOM-Gulf of Maine Version 3 (FVCOM-GOM3) in this study is a circulation model for the US Northeast Coastal Ocean Forecast System, which is nested within the FVCOM-Global model (Chen *et al.*, 2011). The model domain covers the NAS from the Scotian Shelf to the MAB, and adjacent slope and basin regions (Figure 1). The horizontal grid resolution ranges from 10 km in the deep basins and flat shelves to 0.5 km in coastal regions and topographically complex regions such as the shelf break, channels, and canyons. The vertical grid is discretized into 45 layers using a hybrid terrain-following coordinate (Chen *et al.*, 2011). To support the quality of model products, FVCOM-GOM3 also assimilates mooring and ship measurements of temperature and salinity profiles using the optimal interpolation method and mooring current profiles using the nudging method (Chen *et al.*, 2009). The physical outputs of this model have been validated through comparisons with available hy-

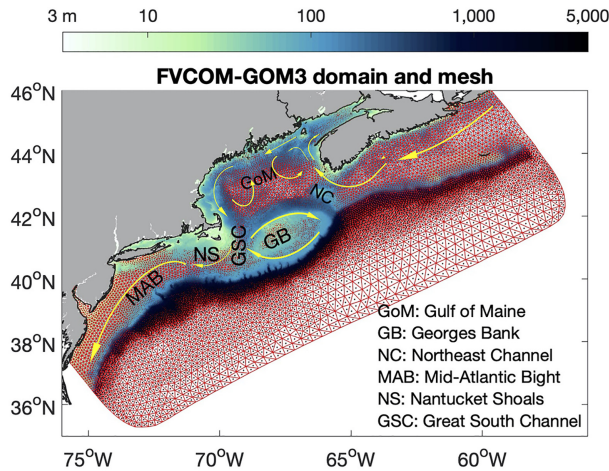


Figure 1. FVCOM model domain and unstructured triangular mesh (red lines) for the Northwest Atlantic Shelf. The colour of cell centres (dots) represents water depth. Yellow arrows represent surface circulation patterns over the shelf.

drographic observations. The model–data comparisons include (1) water elevations at tidal gauges (Chen et al., 2011; Sun et al., 2013), (2) temperature and salinity in the water column (Li et al., 2015), and (3) surface currents measured by coastal ocean dynamics application radar from 2000 to 2008 (Sun et al., 2016). These comparisons demonstrate that the model captures tidal- and shelf-break density fronts, residual gyres, wind-driven upwelling, buoyancy-driven river plumes, the Gulf Stream–shelf interaction, and volume and mass transports entering the GoM over the Scotian Shelf from the upstream. Hourly mean outputs of this hydrodynamic model were downloaded from the data server of the University of Massachusetts Dartmouth (<http://fvcom.smast.umassd.edu>) to drive the marine food web model simulations in an offline coupling mode. The two successive hourly physical fields (e.g. current velocities in different directions, short wave radiation, and water temperature) are linearly interpolated to the time step of the marine food web model (i.e. 120 s). The 3D transport equation is recalculated in two steps based on the interpolated physical fields to ensure the mass conservation of biological tracers in the food web model. In the first step, the biological variables are calculated using the advection and horizontal diffusion terms along with the biogeochemical source/sink terms. The advection terms are calculated using a second-order upwind scheme. In the second step, the vertical diffusion term is discretized and calculated using an implicit scheme following Chen et al. (2003).

Marine food web model

An intermediate-complexity nutrient-phytoplankton-zooplankton-detritus (NPZD) model was implemented to simulate lower trophic level food web dynamics on the NAS. The nitrogen-based model structure is modified from a nine-component global ecosystem model (Stock and Dunne, 2010) by adding a mesozooplankton group (Song et al., 2010, 2011; Figure S1). The ten functional groups in the model include dissolved inorganic nitrogen (DIN), small phytoplankton (SP), large phytoplankton (LP), small zooplankton (SZ), mesozooplankton (MZ), large zooplankton (LZ), bacteria (BAC), labile small detritus (SD_L), semi-labile small detritus (SD_S), and large detritus (LD). Model parameters

were tuned to better fit the NAS ecosystem. The vertical settling fluxes of LD, SP, and LP are resolved using a piecewise parabolic method and a weighted essentially non-oscillatory scheme. Due to the importance of resuspension in LD dynamics at the bottom, one sediment layer for LD is applied to store the total amount of LD settled on the seabed. The remineralization rate of LD in the sediment layer is specified as zero. The resuspension flux of LD (E_{LD}) is estimated based on current-induced bottom shear stress following Ariathurai and Arulanandan (1978), and E_{LD} can directly influence the concentration of LD in the bottom water layer. Zooplankton grazing terms in the model utilize Holling type II formulation if only one type of prey is available. When multiple types of prey exist, the switching response of grazing is included (Gentleman et al., 2003; Stock et al., 2008; Stock and Dunne, 2010). The fractions of MZ and LZ consumed by higher predators (HP) are based on their relative abundance and HP grazing rate following the switching response of grazing as well (Stock and Dunne, 2010). To simplify model processes, the atmospheric deposition of nutrients at the surface and denitrification processes at the bottom boundary are not considered, although some prior studies have suggested those processes might be important in nitrogen cycling during certain time periods (Fennel et al., 2008; Friedrichs et al., 2019).

The focus of this study is phytoplankton dynamics and size composition, so we only show the growth rate equations for SP and LP. The role of zooplankton in the NAS ecosystem is beyond the scope of this paper and will be assessed in our follow-up studies. Readers are referred to Geider et al. (1997), Stock and Dunne (2010), and Song et al. (2011) for more details regarding the model's structure and equations. The phytoplankton growth rates of SP (μ_{SP}) and LP (μ_{LP}) are limited by temperature ($f(T)$), nutrient concentration ($g(N)$), and light availability for photosynthesis ($h(I)$),

$$\mu_{SP(LP)} = \frac{\mu_{SP(LP),max}}{1 + \zeta_{SP(LP)}} \times f(T) \times g(N) \times h(I) - meta_{SP(LP)} \times f(T), \quad (1)$$

$$f(T) = (Q_{10,SP(LP)})^{\frac{T-20}{10}}, \quad (2)$$

$$g(N) = \frac{N}{K_{N,SP(LP)} + N}, \quad (3)$$

$$h(I) = 1 - \exp\left(-\frac{\alpha_{SP(LP)} \times I \times \theta_{SP(LP)}}{\mu_{SP(LP),max} \times f(T) \times g(N)}\right). \quad (4)$$

Here $\mu_{SP(LP),max}$ and $meta_{SP(LP)}$ are maximum nutrient-saturated growth rate and basal metabolism rate of phytoplankton at the reference temperature (20°C), respectively. $Q_{10,SP(LP)}$ is phytoplankton temperature dependence coefficient. $K_{N,SP(LP)}$ represents half saturation coefficient for nutrient-limited growth. I is the incoming shortwave radiation flux for photosynthesis at the centre of each grid. $\alpha_{SP(LP)}$ is the initial slope of the photosynthesis–irradiance (P-I) curve. $\zeta_{SP(LP)}$ is the fraction of biosynthesis cost. Chlorophyll to carbon ratio, $\theta_{SP(LP)}$, is defined following Geider et al. (1997). All model parameters mentioned above are described in Table S1. It is worth noting that silicate is another important limiting nutrient for LP (i.e. diatom) in our study region (e.g. Townsend et al., 2006, 2010). Given roughly equal proportions of nitrate and silicate taken up by diatoms and relatively lower concentrations of silicate than nitrate in the GoM, silicate is depleted earlier and limits the growth of diatoms in the centre of the GoM (Townsend et al., 2006). In coastal regions, however, the depletion of nitrate during the spring bloom limits the growth of phytoplankton due

to silicate-rich terrestrial discharge (Schoudele, 1996). The model implemented for this study follows our earlier model configuration without silicate cycle (Stock and Dunne, 2010; Song *et al.*, 2011). This caveat needs to be taken into consideration when interpreting the model results, especially for the deep central GoM region.

Observational data sets

To assess our model's hindcast skills in reproducing phytoplankton climatology and seasonality, we compiled both ship-based measurements and satellite data for model-observation comparison. Historical *in situ* chlorophyll measurements of small-sized nanoplankton (2–20 μm) and large-sized netplankton (20–300 μm) were retrieved from a total of 182 cruises (August 1976–January 1988) during the Marine Resources Monitoring, Assessment & Prediction (MARMAP) Program of the National Oceanic and Atmospheric Administration (NOAA). The details of sample acquisition and laboratory processing procedures were described in O'Reilly and Zetlin (1998). Given MARMAP's monthly sampling frequencies and strong mixing over the top 10 m (Tian *et al.*, 2014; Li *et al.*, 2015), we computed bimonthly climatology (January–February, March–April, May–June, July–August, September–October, and November–December) of large vs. small phytoplankton size ratio by averaging observed values every 0.5° grid between 0 and 10 m depths. In addition, the bimonthly chlorophyll composites of GlobColour merged satellite products (<http://www.globcolour.info>) from 1998 to 2014 were interpolated to the model grid and compared with the simulated surface chlorophyll climatology to demonstrate the bimonthly patterns of model results (Maritorena *et al.*, 2010). It is worth noting that this bimonthly comparison between model results and satellite images was not for the assessment of detailed bloom timing due to the coarse temporal resolution. An EOF analysis with a higher temporal resolution (8-day composite) was conducted to evaluate more detailed timing variability patterns across the entire model domain. Field observations of nitrogen ($\text{NO}_3 + \text{NO}_2$) and chlorophyll were extracted from the Gulf of Maine Region Nutrient and Hydrographic Database (<http://grampus.umeoce.maine.edu/nutrients>), a combination of several global, and regional datasets (Rebuck and Townsend, 2014).

Sensitivity tests

The response of phytoplankton growth rate to temperature is crucial in simulating marine primary productivity, and its parameterization directly impacts the model's capacity in reproducing ocean ecosystem dynamics under the rapid global climate change. Our model utilizes a Q_{10} relationship to represent the response of phytoplankton growth rate to temperature variation (see Equation 2). The maximum growth rate of phytoplankton increases (decreases) with the elevation of $Q_{10, SP(LP)}$ above (below) the reference temperature (20°C in this study) and vice versa (Figure S2). Q_{10} was specified as 2.0 in our benchmark run following previous studies (Ji *et al.*, 2008b; Stock and Dunne, 2010; Song *et al.*, 2011). However, estimations of Q_{10} based on measurements suggested that many factors (e.g. species, physiological changes, temperature interval, genotypic difference) could cause significant deviations from 2.0 (Eppley, 1972; Sherman *et al.*, 2016). Here, we increased/decreased $Q_{10, SP(LP)}$ by 0.3 and 0.6, respectively, and conducted one-year simulations in

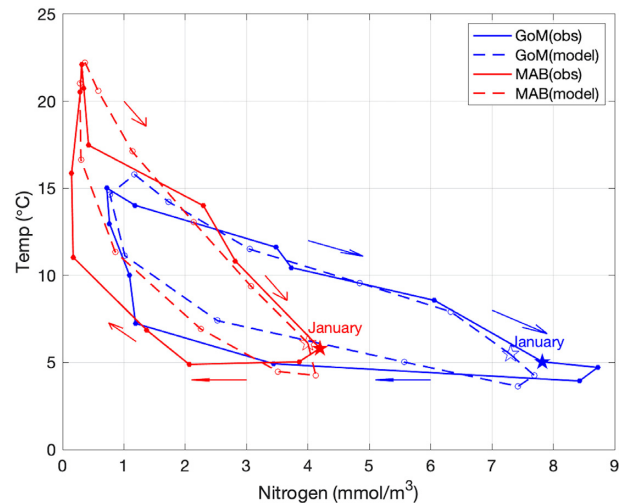


Figure 2. Annual cycle of temperature versus nitrogen concentration over the top 10 m in the GoM (blue) and the MAB (red). The solid lines are based on monthly observations and the dashed lines are based on model results. The stars represent January and circles represent other months. The direction of the annual cycle is clockwise.

1978 to examine its importance in the seasonality of phytoplankton dynamics over the NAS.

Results

Nitrogen dynamics in the GoM and the MAB

We compared simulated monthly averaged nitrogen concentration over the top 10 m with observations in the GoM and the MAB (see Figure S3 for locations). Our model reasonably reproduced the temporal variability of surface nitrogen, i.e. high in winter ($> 5 \text{ mmol m}^{-3}$) and low in summer ($< 2 \text{ mmol m}^{-3}$) (Figure S4). The time series of simulated nitrogen was well correlated with measurements in the GoM ($r = 0.85$; $\text{RMSE} = 1.49$) and the MAB ($r = 0.68$; $\text{RMSE} = 1.86$), indicating the robust performance of our model in reproducing the seasonality of surface nitrogen on the NAS (Figure S4). The simulated deep nitrogen below 100 m was also comparable to the field observed concentrations without a strong seasonality (Figure S5).

To better demonstrate the seasonality of nitrogen concentration, the annual cycle of monthly mean temperature versus surface nitrogen concentration is shown in Figure 2. The comparison between model and observations suggested that our model well captured the seasonal variation of nitrogen, which was strongly linked to thermal regime shifts among different seasons. The annual cycle was similar in the GoM and the MAB: nitrogen reached the highest level from January to March and the lowest level from May to September. The most dominant nitrogen difference between the GoM and the MAB was found in winter, during which nitrogen concentration in the MAB was about 4 mmol m^{-3} lower than that in the GoM. In the summer season, the nitrogen concentration difference between the two regions was less than $\sim 1 \text{ mmol m}^{-3}$, while the water temperature differed by up to 8°C .

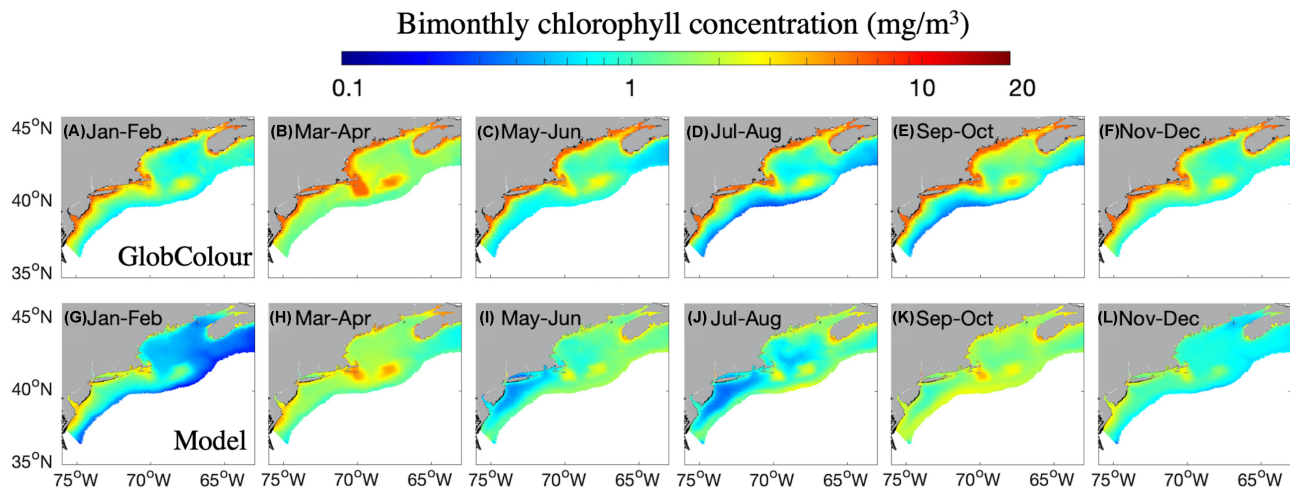


Figure 3. Bimonthly chlorophyll concentration comparison between GlobColour (upper panels) and model results over the top 10 m (lower panels). The cutoff water depth is 1000 m.

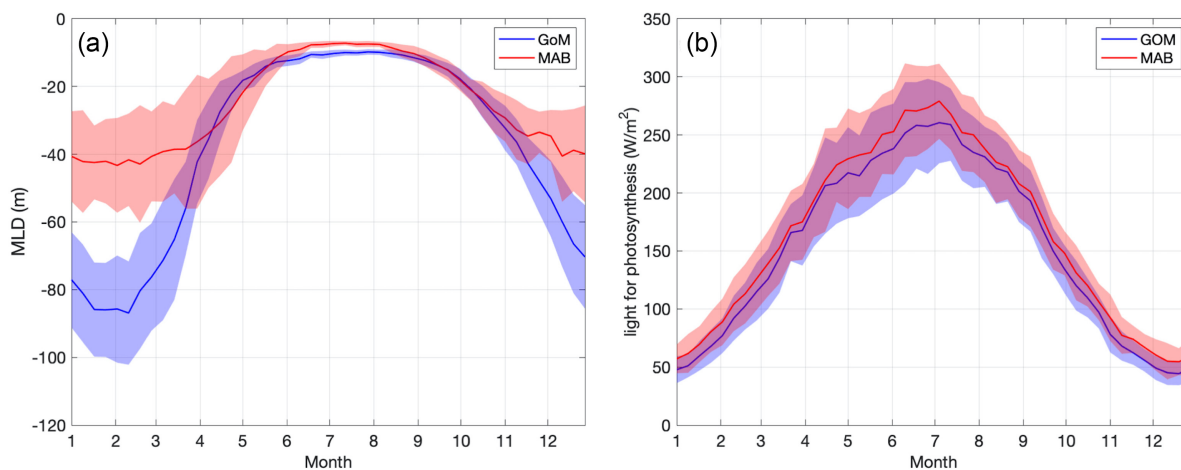


Figure 4. Spatial mean of mixed layer depth (a) and light for photosynthesis (b) climatology (8-day composite) in the GoM and the MAB. Shaded areas represent one standard deviation.

Spatiotemporal variability of surface chlorophyll

We compared the bimonthly GlobColour-derived chlorophyll composites with simulation results (chlorophyll from both phytoplankton size classes combined) to assess the model's performance in reproducing the surface phytoplankton dynamics (Figure 3). Over the entire study area, the chlorophyll concentration was higher along the coast due to vertical mixing in shallow areas and decreased gradually offshore. Our simulated chlorophyll concentration in coastal regions was overall lower than the satellite results (Figure 3). The offshore chlorophyll hotspot on Georges Bank had concentrations exceeding 1 mg m^{-3} year-round. Shallow water depth, strong tidal mixing, and offshore nutrient supply jointly contributed to the formation of this productivity hotspot (Hu et al., 2008; Ji et al., 2008a). The seasonality of chlorophyll was well reproduced in our simulation: the spring bloom was found in March and April when the chlorophyll concentration reached more than 1 mg m^{-3} on the shelf in both the GoM and the MAB (Figure 3b and h). The appearance of spring bloom corresponded with water warming, increased light for photosynthesis, stratification, and high surface nitrogen concentration ($> 1 \text{ mmol m}^{-3}$), and the remarkable decrease

of nitrogen in March and April was caused by rapid phytoplankton growth and weakened nutrient replenishment associated with stratification (Figures 2 and 4a). From May to August, the decreased chlorophyll over the NAS resulted from nitrogen limitation and reduced chlorophyll-to-carbon ratio associated with high light levels, despite higher temperature and favourable light condition for phytoplankton growth (Figures 3c, d, i, j, and 4b). The secondary bloom took place in September and October due to nitrogen replenishment associated with enhanced vertical mixing (Figures 2, 3e, k, and 4a). From November to February, high nitrogen concentration (GoM: $6\text{--}9 \text{ mmol m}^{-3}$; MAB: $2\text{--}4 \text{ mmol m}^{-3}$), low water temperature (GoM: $4\text{--}8^\circ\text{C}$; MAB: $5\text{--}11^\circ\text{C}$), and low light levels indicated the NAS shifted to a light- and temperature-limited ecosystem (Figures 2, 3a, f, g, l, and 4b).

We further evaluated the model's performance by conducting empirical orthogonal function (EOF) decomposition to the 8-day composite of chlorophyll climatology based on both model results and the GlobColour data (Figure 5). Prior to the EOF decomposition, the climatology was normalized by subtracting its temporal mean and dividing the standard deviation of each model node

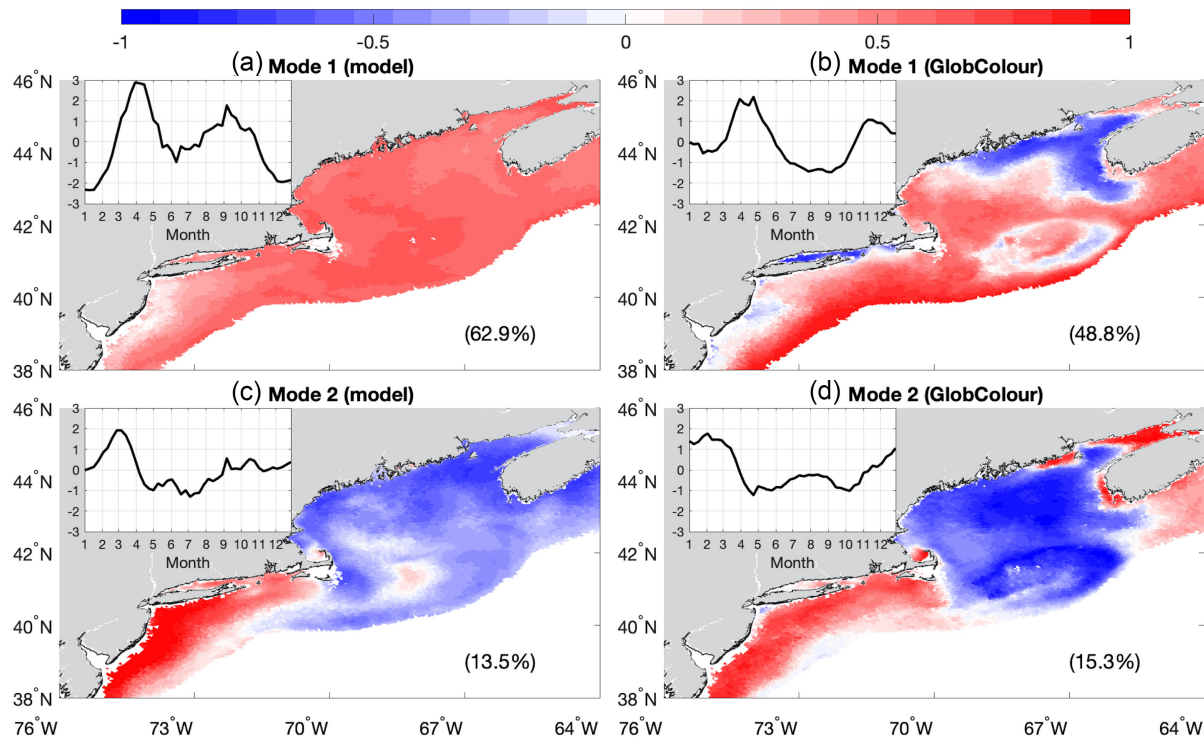


Figure 5. Spatial patterns of EOF analysis based on the normalized modelled (left-hand column) and GlobColour (right-hand column) surface chlorophyll concentration with the corresponding time series (upper left-hand of each panel) and the percentage of variability explained by each mode (lower right-hand corner of each panel). The upper two panels represent the first mode and the lower two panels represent the second mode, respectively.

following Yoder *et al.* (2002). The first modes of both model (62.9% of the total variance) and GlobColour (48.8% of the total variance) suggested that chlorophyll over most regions varied synchronously (Figure 5a and b), although the negative pattern in the eastern GoM GlobColour data was not seen in our model. The time series of the first mode illustrated the canonical seasonality of chlorophyll with a primary bloom in winter–spring and a secondary bloom in fall (Figure 5a and b). In the first mode, the simulated secondary bloom was about one month earlier than the satellite data. The discrepancy in the timing of secondary bloom could be caused by the overestimated surface nitrogen concentration in September in the GoM (observation: 1.2 mmol m^{-3} ; model: 1.8 mmol m^{-3}) and the MAB (observation: 0.4 mmol m^{-3} ; model: 0.7 mmol m^{-3}) (Figure 2). The second mode accounted for 13.5 and 15.3% of the total variance in model results and GlobColour data, respectively. The corresponding spatial patterns showed that chlorophyll in the GoM and the MAB were out of phase: a negative pattern was prevalent over the entire GoM, while a positive pattern dominated the MAB (Figure 5c and d). The boundary of these two opposite patterns located over the Nantucket Shoals along the 70° W meridian. The time series of the second mode demonstrated winter maxima and summer minima in the MAB, while the opposite temporal variation was found in the GoM (Figure 5c and d).

To investigate what was responsible for the spatial heterogeneity of surface chlorophyll on the NAS, we estimated water temperature and nitrogen climatology at the surface using the 8-day composite of our model in the GoM and the MAB, respectively. It is noteworthy that the surface photosynthetic available radiation (PAR) con-

tributes little to the spatial heterogeneity of chlorophyll between the GoM and the MAB, especially when compared with the differences of temperature and nutrient in these two regions (Figures 4b, 6a and b). Water temperature and nitrogen concentration were out of phase by 6 months in both regions: temperature peaked in summer and minimized in winter, whereas nitrogen concentration was low in summer and high in winter (Figure 6a and b). Based on our modelled water temperature and nitrogen concentration, we derived the annual cycle of $f(T)$ and $g(N)$ for SP and LP in different regions to quantitatively estimate the relative importance of nutrient and temperature in phytoplankton growth (see Equations 2 and 3). In our model, $g(N)$ and $f(T)$ jointly limited the growth of phytoplankton, and Liebig's law of minimum was not applied in this study. In the GoM, the $g(N)$ of SP was around 0.9 with very limited temporal variation. The $f(T)$ of SP in the GoM, however, shifted from 0.38 in winter to 0.81 in summer, and it was lower than $g(N)$ year-round, implying the growth of SP in the GoM was more limited by temperature than by nitrogen (blue line in Figure 6c). Owing to lower nitrogen concentration and higher temperature in the MAB (Figure 6a and b), the impact of limited nitrogen to SP growth surpassed that of temperature ($g(N) < f(T)$) from late spring to the end of summer (red line in Figure 6c). Since we employed the same Q_{10} but higher half-saturation coefficient (K_n) for LP, the $f(T)$ of SP and LP were identical, but the $g(N)$ of LP was lower than that of SP. Compared with SP, the growth of LP was more sensitive to the variation of nitrogen, especially in summer when nitrogen concentration was less than 2 mmol m^{-3} (Figure 6b and d). LP's $g(N)$ in the GoM ranged from 0.56 to 0.91, which was lower than its $f(T)$ from

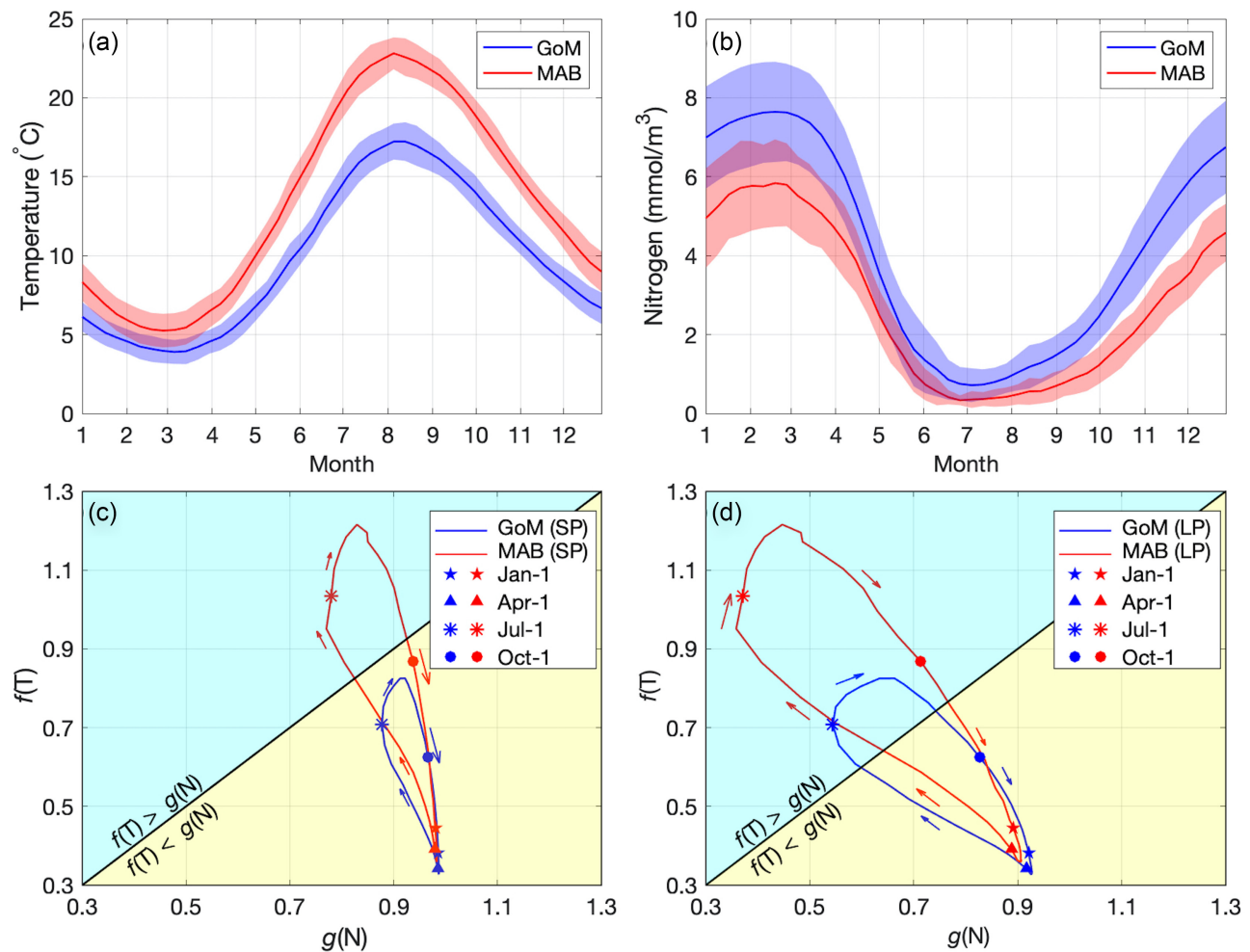


Figure 6. The upper two panels show spatial mean of water temperature (a) and nutrient (b) climatology (8-day composite) over the top 10 m in the GoM and the MAB. Shaded areas depict one standard deviation. The lower two panels represent annual cycle of nutrient limit term $g(N)$ versus temperature limit term $f(T)$ for small phytoplankton (SP; panel c) and large phytoplankton (LP; panel d). In cyan area, nutrient limitation outweighs temperature limitation ($f(T) > g(N)$). In yellow area, the nutrient limitation is weaker than temperature limitation ($f(T) < g(N)$). The direction of the annual cycle is clockwise.

late spring to late summer (blue line in Figure 6d). In the MAB, the duration of $f(T) > g(N)$ was even longer starting from mid-spring until early fall (red line in Figure 6d). In general, the intrinsic growth rate of phytoplankton in the GoM was more limited by temperature than by nitrogen, while relatively lower nitrogen concentration and higher water temperature in the MAB contributed to stronger nutrient limitation on phytoplankton growth. Compared with the second mode of chlorophyll EOF analysis (Figure 5c and d), the seasonality of temperature and nitrogen and their limiting effects roughly matched the second mode of EOF analysis in the GoM and the MAB, respectively. In the GoM, low temperature strongly limited the growth of phytoplankton in the cold season, resulting in the shift of two blooms in the canonical seasonality of phytoplankton (the first mode of EOF analysis) towards the warm season with a delayed spring bloom and an advanced fall bloom. In the MAB, the increased importance of nutrient limitation in the warm season and relatively high temperature in late fall and winter shifted the bloom timings towards the opposite direction (an earlier primary bloom in winter and a later secondary bloom in fall).

The seasonality of phytoplankton size structure

Both model results and the MARMAP dataset illustrated a strong seasonality of phytoplankton size structure over the NAS (Figure 7). In January and February, LP was abundant in coastal regions (LP fraction > 70%), while SP dominated offshore and the centre of the GoM (Figure 7a and g). In March and April, LP became dominant on the NAS, reflecting the importance of diatoms in the winter-spring phytoplankton bloom (Figure 7b and h). Subsequently, the dominant phytoplankton type shifted from LP to SP rapidly over the entire shelf until the end of August, when LP only dominated sporadically along the coast of the GoM and over Georges Bank (Figure 7c, d, i, and j). From September to December, the percentage of LP increased moderately with minor changes in spatial distribution pattern (Figure 7e, f, k, and l).

We further compared the simulated monthly LP fraction ($\frac{LP}{LP+SP} \times 100\%$) with the observations in the GoM and the MAB, respectively (Figure 8). High correlation coefficients (GoM: $r = 0.83$; MAB: $r = 0.90$) suggested our simulated phytoplankton size structure matched that of the observations, although the LP fraction appeared to be overestimated in the GoM throughout the

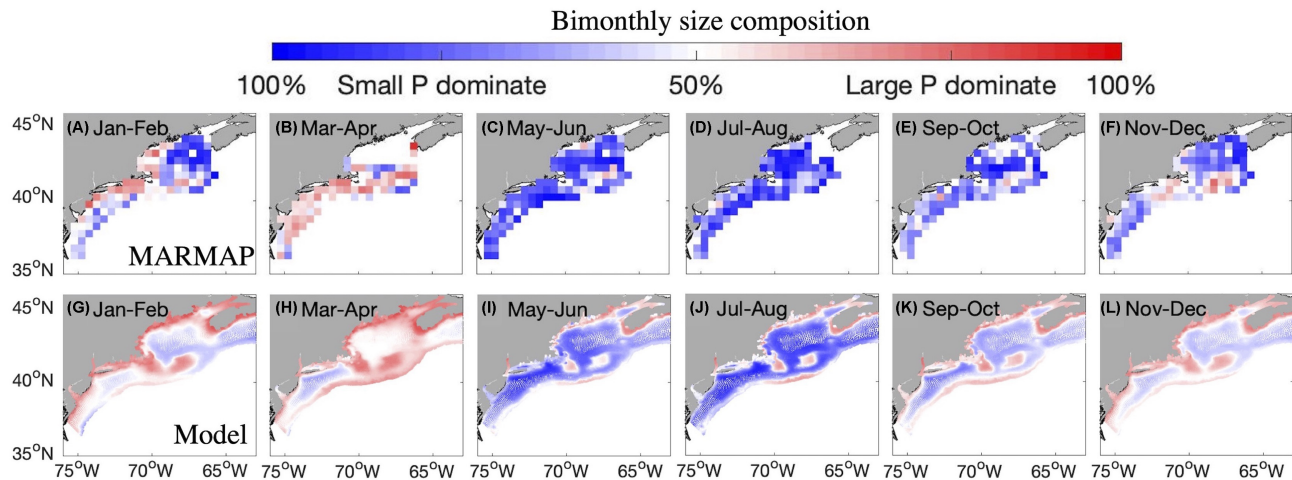


Figure 7. Bimonthly phytoplankton size structure comparison between MARMAP dataset (upper panels) and model results over the top 10 m (lower panels). The cutoff water depth is 1000 m.

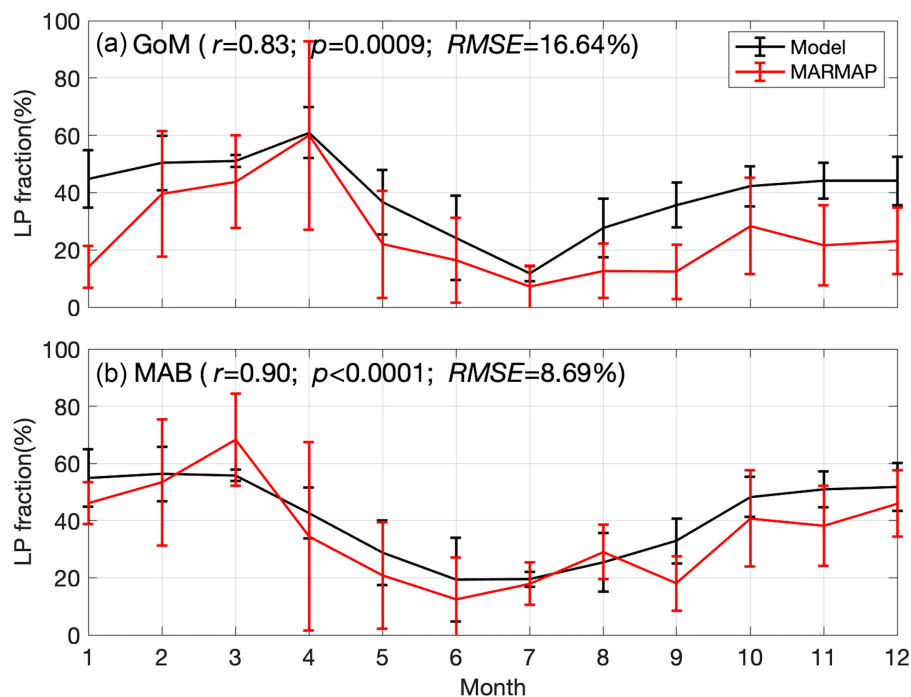


Figure 8. Modelled (black) and MARMAP (red) monthly time series of large phytoplankton (LP) fraction in the GoM (a) and MAB (b). Error bars indicate one standard deviation.

year (Figure 8). The LP fraction in the GoM increased gradually from January to April, and the peak value ($\sim 60\%$) was followed by a sharp decrease until July (Figure 8a). After that, the LP fraction increased slightly and fluctuated around 30% until the end of the year. In the MAB, the temporal variation of LP fraction was overall similar to that in the GoM (high in the cold season and low in the warm season), while both the peak and trough of LP fraction appeared about one month in advance (Figure 8b).

EOF results of bottom LD and chlorophyll

To examine the links between pelagic production and exported organic materials reaching the seafloor, we applied EOF analysis to

8-day composites of chlorophyll and LD climatology in the bottom layer to reveal their spatiotemporal patterns (Figure 9). For bottom chlorophyll, the spatial patterns of the first two modes were very similar to those of surface chlorophyll: positive pattern dominated the entire shelf in the first mode except for the deep central GoM, and opposite patterns between the GoM and the MAB were found in the second mode (Figure 9a and c). For bottom chlorophyll, the first EOF mode did not have a fall peak. The first two modes of bottom LD, however, had very different spatiotemporal patterns compared with the corresponding modes of chlorophyll (Figure 9b and d). The GoM and the MAB had opposite patterns in the first mode of bottom LD, and the corresponding time series had a sinusoidal annual cycle (Figure 9b). The spatial heterogeneity

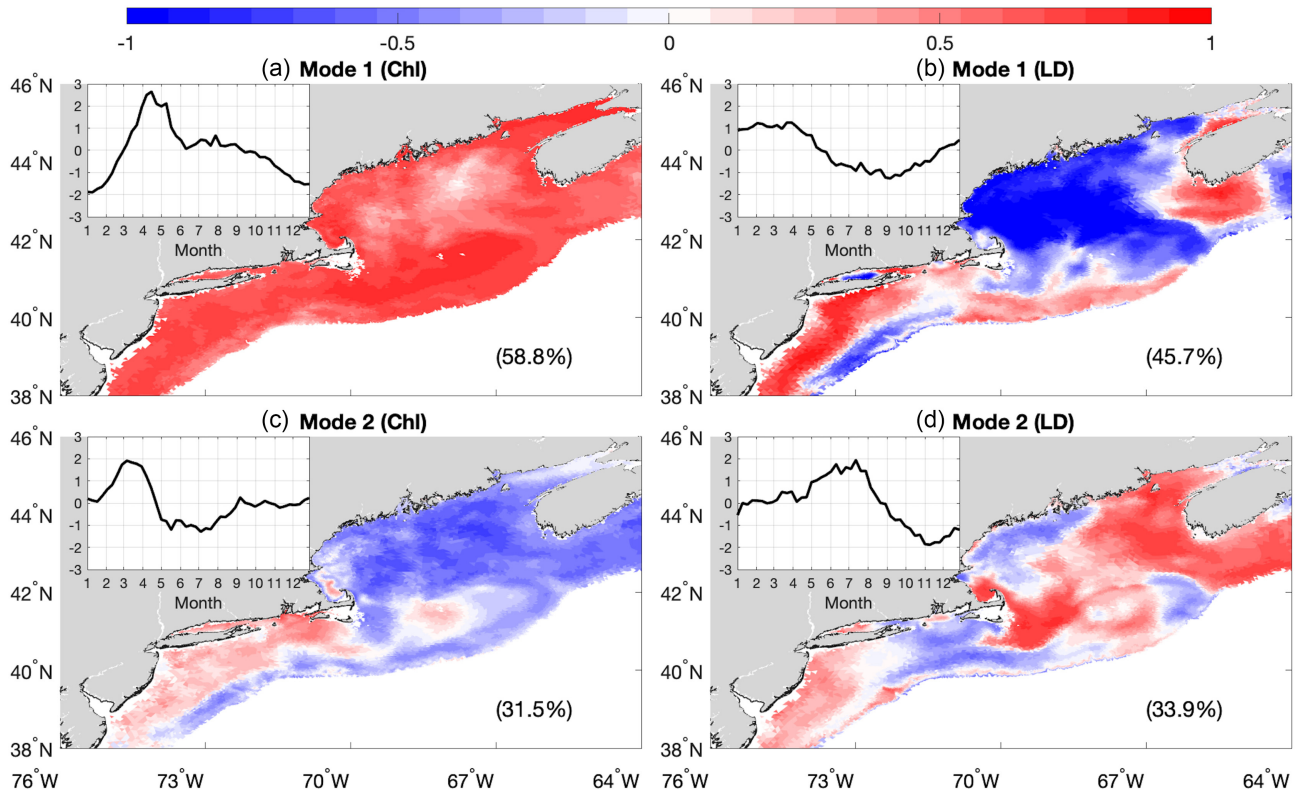


Figure 9. Spatial patterns of EOF analysis based on the modelled chlorophyll concentration (left-hand column) and large detritus concentration (right-hand column) at the bottom with the corresponding time series (upper left-hand of each panel) and the percentage of variability explained by each mode (lower right-hand corner of each panel). The upper two panels represent the first mode and the lower two panels represent the second mode, respectively.

in the second mode of bottom LD was even greater over the NAS (Figure 9d).

Thermal sensitivity of phytoplankton dynamics

To investigate the sensitivity of phytoplankton dynamics to temperature and to explore how Q_{10} parameterizations can affect modelled phytoplankton's seasonality, we compared the time series of chlorophyll concentration in the top 10 m between the benchmark run and sensitivity test runs (Figure 10). In the GoM, the major discrepancies among different cases were detected during both the spring and fall blooms, while minor difference in chlorophyll concentrations occurred during the rest of the year (Figure 10a). In the MAB, only the spring bloom was sensitive to changes in Q_{10} (Figure 10b). To quantitatively estimate the impacts of Q_{10} on phytoplankton dynamics, we derived the timing and magnitude of blooms in the GoM and the MAB following Ji et al. (2007). As Q_{10} increased from 1.4 to 2.6, the peak of the spring bloom in the GoM was delayed from mid-March to mid-May with a remarkable magnitude decrease from 6.5 to 1.8 mg m⁻³ (Figure 10c and d). The spring bloom magnitude declined with higher Q_{10} in the GoM because climatological mean temperature in the GoM was always lower than the reference temperature (20°C; Figure 6a), below which higher Q_{10} value corresponded to lower phytoplankton growth rate in the Q_{10} model (Figure S2). In the MAB, the timing of the spring bloom was insensitive to the variation of Q_{10} , while its magnitude decreased markedly from 5.6 to 1.8 mg m⁻³ as Q_{10} increased (Figure 10c and d). The timing of the fall bloom in the two areas advanced about 15

days with slightly reduced magnitude as Q_{10} increased from 1.4 to 2.6 (Figure 10c and d). Overall, a lower Q_{10} value contributed to an earlier spring bloom and a later fall bloom with enhanced magnitude, and phytoplankton dynamics in the GoM was more sensitive to Q_{10} variations than that in the MAB.

Discussion

Spatial heterogeneity of thermohaline structure and phytoplankton dynamics on the NAS

In our study region, the GoM and the MAB have different thermohaline structures (Li et al., 2015). In the MAB, water temperature is higher than that in the GoM due to the combination of strong surface heating, exchange with warm slope water, and the absence of direct cold water inflow from subpolar regions (Loder, 1998); The nearshore salinity in both regions is significantly influenced by terrestrial freshwater discharge, while low-salinity water inflow from higher latitude further enhances freshening in the GoM during winter–spring season (Mountain and Manning, 1994). The difference of thermohaline structures between the GoM and the MAB results in a distinct annual cycle of stratification in these two regions: earlier and stronger stratification in the MAB is thermally dominated through a large portion of the year, whereas haline control strengthens in the GoM (Li et al., 2015). Many studies have confirmed that surface nutrient replenishment is strongly correlated with mixing (e.g. Townsend, 1998; Townsend et al., 2010). As stated above, different surface nutrient regimes and water temperature be-

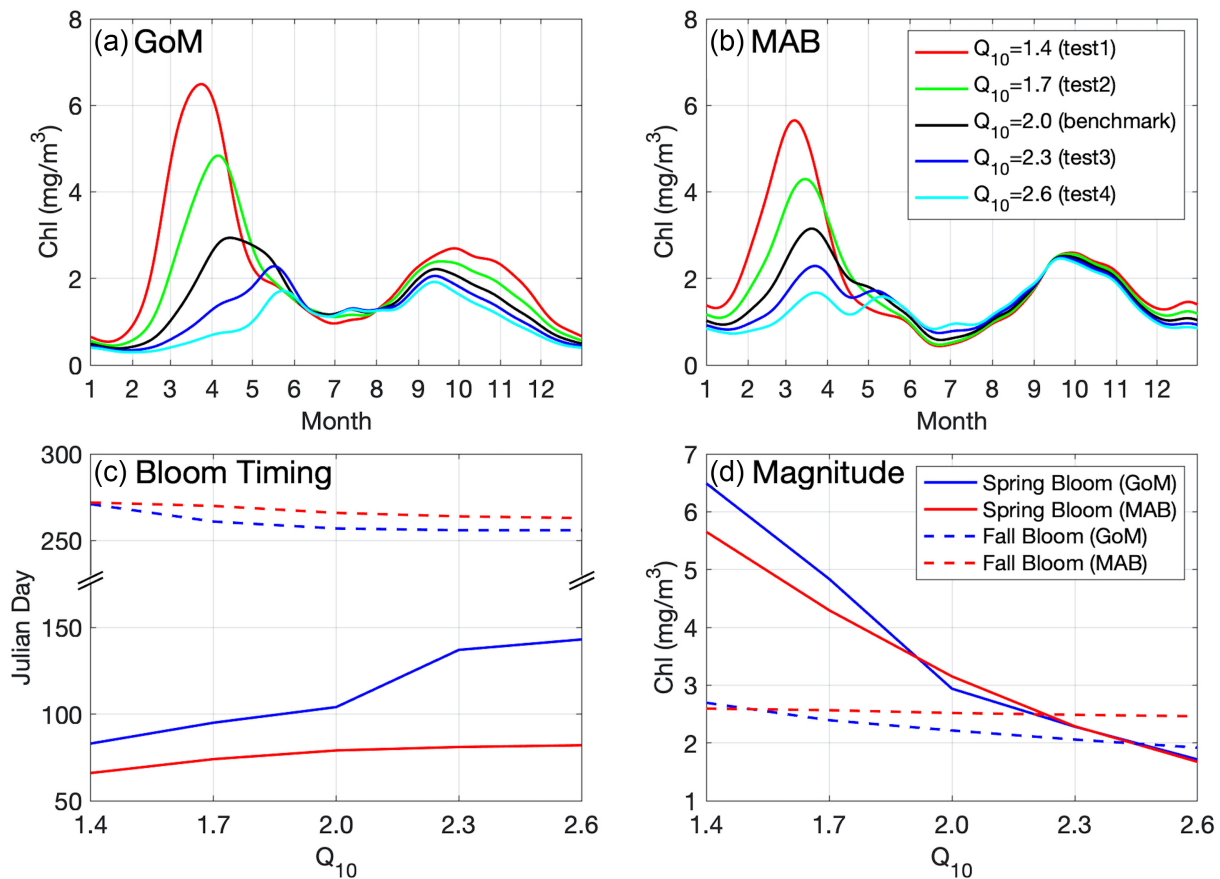


Figure 10. Comparison of spatial averaged chlorophyll concentration over the top 10 m between the benchmark run (black line) and sensitivity tests with different Q_{10} in the GoM (a) and the MAB (b). A Gaussian smoothing was applied to model results following Ji *et al.* (2007) for detecting bloom timing (c) and magnitude (d).

tween the GoM and the MAB are responsible for the spatial heterogeneity of phytoplankton dynamics between the two regions: in the GoM, relatively high nutrient concentration due to strong mixing and low water temperature result in weaker limitation of nutrient but stronger limitation of temperature for phytoplankton growth. On the other hand, stratification-induced lower nutrient supply and warmer water in the surface mixed layer of the MAB contribute to more significant nutrient limitation. Chlorophyll concentration in the GoM reaches a maximum in spring, while the primary bloom on the MAB shelf occurs earlier in winter. The spatial heterogeneity of phytoplankton dynamics might also exist between the eastern GoM and western GoM (Figure 5b). Compared with surface chlorophyll observations, the spring bloom cannot be detected in the GlobColour satellite data in the eastern GoM (Figures S6 and S7), and this bias contributes to the opposite pattern in the first EOF mode of the satellite data (Figure 5b). The quality of GlobColour data in the eastern GoM might be compromised by coloured dissolved organic matter and resuspended sediment (Butman *et al.*, 2014; Balch *et al.*, 2016). The spring bloom in the eastern GoM is reproduced in our model results, whereas the simulated spring bloom happens earlier with relatively low magnitude compared to field measurements (Figures S6 and S7). Therefore, the difference in the eastern GoM between model and satellite in the first mode of EOF analysis can be ascribed to the errors in both simulation results and satellite products.

In the cross-shelf direction, both model and satellite images demonstrate that chlorophyll concentration in the GoM decreases from shallow coastal regions to deep basins, although the cross-shore gradient of model results is relatively low because of the underestimation of simulated chlorophyll nearshore (Figure 3). The discrepancy can be a result of overestimated chlorophyll concentration in satellite data due to high coloured dissolved organic matter and sediment concentrations nearshore, or underestimated chlorophyll concentration in simulation results due to the improperly resolved phytoplankton-grazer linkages and the absence of large, chain-forming coastal large phytoplankton in our model (Hyde *et al.*, 2007; Van Oostende *et al.*, 2018). Over the MAB, however, the cross-shelf gradient of chlorophyll is more complicated due to strong interactions between shelf and slope waters (Malone *et al.*, 1983). The canonical viewpoint suggests a dramatic decrease of chlorophyll concentration from the MAB shelf to slope (Malone *et al.*, 1983; Yoder *et al.*, 2001), whereas high chlorophyll concentration on the shelf break has been recorded by both satellite data and field measurements (Ryan *et al.*, 1999; Mouw and Yoder, 2005). Unlike the winter bloom over the MAB shelf, the chlorophyll bloom over the shelf break regions occurs in spring with lower magnitudes (Xu *et al.*, 2011). The cross frontal water exchange, due to many factors (e.g. frontal instability, wind, warm-core rings, and shelf break upwelling), contributes to nutrient delivery to the euphotic zone and stimulates chlorophyll enhancement in the shelf break region

(Ryan et al., 1999). This offshore bloom can be found in our simulation results as well (Figure 3i, j, and k), yet such a feature does not exist in satellite climatology (Figure 3c, d and e). The discrepancy between model and satellite data can be attributed to the model underestimation of zooplankton grazing pressure (Zhang et al., 2013), but more studies are needed to explore the underlying mechanisms.

The spatial heterogeneity of phytoplankton size structure between the GoM and the MAB is strongly related to diatom blooms: the diatom blooms in the GoM and the MAB occur in winter–spring, and the bloom asynchrony results in phytoplankton size structure difference between the two regions (Figure 8). Unlike the winter diatom bloom on the MAB shelf, the bloom over the MAB shelf break occurs in spring and is dominated by small phytoplankton (Ryan et al., 1999). Consequently, the seasonality of phytoplankton size structure over the MAB shelf break is different from the rest of the NAS.

The increase of sea surface temperature in the GoM is reported to be faster than most of the global ocean (Pershing et al., 2015), and future projections suggest this rapid warming will continue (Loder et al., 2015). As suggested by this study, water temperature and nutrient level at the surface are responsible for the spatial heterogeneity of phytoplankton dynamics between the GoM and the MAB. It then begs the question of will phytoplankton dynamics in the GoM become more similar to that in the MAB as the GoM warms in the upcoming decades. If the temperature effect on growth rate is the dominant factor regulating the abundance of phytoplankton, the increasing thermal regime similarities between the GoM and the MAB can potentially reduce the spatial heterogeneity of phytoplankton seasonality (Shearman and Lentz, 2010). However, this direct temperature effect can be confounded by the surface nutrient dynamics regulated by stratification, which is more thermally regulated in the MAB compared to the haline-controlled GoM during the winter–spring bloom season (Li et al., 2015). Both satellite and model results indicate the importance of freshening in winter–spring bloom timing and magnitude (Ji et al., 2007, 2008b). Besides, the increasing similarity in the surface thermal regimes between the GoM and the MAB might not result in similar vertical stratification patterns. Warming over the NAS can be ascribed to both surface heating associated with atmospheric warming and lateral advection at depth, which have different impacts on the intensity of stratification (Shearman and Lentz, 2010; Chen et al., 2014). Consequently, vertical stratification and related surface nutrient–phytoplankton dynamics in the GoM and the MAB can still be distinctive even as their surface thermal regimes become similar under rapid warming.

Impact of warming on phytoplankton dynamics on the NAS

In the context of global climate change, surface water temperature in the NAS ecosystem has been increased markedly over the last several decades, with a warming rate of $\sim 0.26^\circ\text{C yr}^{-1}$ starting from the early 21st century (Belkin, 2009; Shearman and Lentz, 2010; Burrows et al., 2011; Mills et al., 2013). However, a comprehensive understanding of phytoplankton response to rapid warming remains challenging due to the complex physical–biogeochemical interactions and tight coupling between different trophic levels. As ambient water temperature increases, the growth of phytoplankton becomes faster due to the thermal adaptation (Eppley, 1972; Staehr and Birkeland, 2006), and the growth rate becomes more sensitive to temperature variations (Figure S2). By contrast, surface heating-induced stratification reduces surface phytoplankton growth by

constraining nutrient replenishment (Figures 2 and 3; Thomas et al., 2003; Song et al., 2011). Previous studies have suggested low nutrient availability has a strong effect on phytoplankton growth (e.g. Staehr and Birkeland, 2006). In addition, temperature modulates nutrient dynamics via not only stratification, but also biogeochemical processes. Laurent et al. (2016) applied temperature-dependent remineralization rate of particulate organic matter in the diagenetic model and found that the nitrogen dynamics were very sensitive to water temperature. The rates of many other nitrogen pathways (e.g. nitrification, nitrogen fixation) are also strongly correlated with water temperature (Damashek and Francis, 2018), implying the importance of temperature in nitrogen cycling and its potential impacts on phytoplankton growth.

Climate-related warming also regulates the growth of phytoplankton ($\mu_{\text{SP(LP)}}$ in Equation 1) via changing phytoplankton temperature dependence coefficient Q_{10} , which represents the thermal responses of the community and varies greatly with the shift of phytoplankton community composition (Staehr and Birkeland, 2006). Physical conditions such as turbulence and temperature, as well as the nutrient regimes, are the primary factors affecting phytoplankton composition: small phytoplankton, such as dinoflagellates, become dominant when the water column is stable and oligotrophic, while large phytoplankton species (e.g. diatoms) are more common in less stratified and nutrient-rich environments (Margalef, 1978; Pershing and Stamieszkin, 2020). As rapid warming continues over the NAS, longer and stronger thermal stratification will favor the dominance of small phytoplankton (Thomas et al., 2017). Due to the wide range of Q_{10} between phytoplankton species, it is reasonable to speculate that the shift of phytoplankton community composition might affect the value of community Q_{10} . Moreover, the thermal adaptation of phytoplankton alters their physiological features and consequently the Q_{10} values, and such response is usually species-specific (Staehr and Birkeland, 2006). Sherman et al. (2016) estimated the Q_{10} value based on a global database of field measurements and found the optimum apparent Q_{10} was around 1.5, which was lower than the value (2.0) in our study. Our Q_{10} sensitivity tests with low Q_{10} values (tests 1 and 2), however, overestimated chlorophyll concentration dramatically during blooms (Figure 10), implying the Q_{10} in the NAS might greatly deviate from the global mean value. Given the importance of Q_{10} parameterization in simulating phytoplankton dynamics (Figure 10), the variation of community Q_{10} may modulate phytoplankton dynamics in the entire NAS ecosystem.

From a top-down control perspective, climate-related warming manipulates phytoplankton abundance via changing zooplankton dynamics. Our EOF results of surface mesozooplankton are similar to that of chlorophyll, implying a tight coupling between zooplankton and phytoplankton (Figures 5 and S8). The ramifications of climate-induced warming for phytoplankton dynamics on the NAS propagate through the food web in both bottom–up and top-down directions. Due to the simplified structures of most 3D biogeochemical models, they can only partially resolve the influence of temperature on marine ecosystems. Future models need to better resolve thermal responses of important physical–biogeochemical processes in order to improve the model projections of future climate scenarios.

Benthic–pelagic coupling on the NAS

The NAS supports some of the commercially important benthic species (e.g. groundfish, sea scallop, and lobster; Pershing and

Stamieszkin, 2020), and their high production is mainly fueled by the sedimentation of surface organic matter (Griffiths *et al.*, 2017). Thus, understanding benthic–pelagic coupling in our study area can help us gain more insight in developing adaptive fishery management strategies under a rapid changing climate. As suggested by this study, the seasonality of bottom chlorophyll modulated by the settling of surface–subsurface phytoplankton, deep production, and chlorophyll to carbon ratio is overall analogous to that in the surface layer over the entire study area, while the seasonality of bottom chlorophyll in the deep basins of the GoM is very weak. The decoupling between the surface and the bottom chlorophyll concentrations in the deep basins is probably bathymetry–driven: the sinking of phytoplankton from the surface to the bottom takes longer time over the deep basins, allowing a significant loss of phytoplankton due to zooplankton grazing, respiration, aggregation, exudation, and viral lysis, thus weakening the seasonality of bottom chlorophyll and benthic–pelagic coupling. Additionally, there is no detectable bottom chlorophyll increase in fall, possibly due to the slow settling of small phytoplankton that dominate the fall bloom at the surface (Figures 7 and 8). The enhancement of vertical mixing in fall might further contribute to the decrease of phytoplankton settling flux on the NAS (Arin *et al.*, 2002; Ross, 2006).

For LD at the bottom, its opposite spatial pattern in the first mode could be explained by vertical settling and production in the euphotic layer: in the GoM, relatively low productivity throughout the water column (Figure S9) and strong vertical mixing in the cold season result in the reduced LD settling flux to the bottom and the increase of LD upward flux from the bottom to the overlying water (Arin *et al.*, 2002; Ross, 2006). In the warm season, stratification limits the LD mixing from the bottom to the surface, and the enhanced surface production can increase the settling flux of LD from the euphotic layer to the bottom (Figure S9). On the inner shelf of the MAB, both strong stratification in the warm season and shallow water depth shorten the duration of LD settling from the euphotic layer to the bottom and contribute to the coupling between surface production and bottom LD concentration: higher surface production and bottom LD concentration are found in winter and spring, while lower values appear in summer (Figures 5 and 9). The opposite pattern on the outer shelf of the MAB might result from the interactions with slope water (Figure 9b; Townsend *et al.*, 2006; Xu *et al.*, 2011). The spatial heterogeneity in the second mode is likely related to LD resuspension, which is determined by local current fields in our model. On the NAS, LD resuspension due to tidal currents has strong spatiotemporal variations. In the GoM, the intensity of current-induced resuspension decreases gradually from coastal regions to deep basins (Butman *et al.*, 2014). In the MAB, both observations and model results suggest energetic winter storms and hurricanes are the major driving forces of strong resuspension, and the contribution of tidal currents becomes very limited (Miles *et al.*, 2015). Since LD is an important food source for benthic organisms, the prominent difference between surface productivity and bottom LD suggests that the pelagic and benthic layers are at least partially uncoupled. It is worth noting that our model, like many 3D biogeochemical models, cannot comprehensively resolve LD resuspension and other benthic–pelagic coupling processes, whose importance in organic matter distribution and nutrient cycling has been emphasized in recent numerical studies (e.g. Laurent *et al.*, 2016; Moriarty *et al.*, 2018). Future modelling efforts should include the dynamics of benthic–pelagic coupling for the NAS ecosystem.

Model limitations and future work

Although our model results provide valuable insights into the seasonality of phytoplankton dynamics in the NAS and driving mechanisms for its spatial heterogeneity, this model has some limitations and warrants further improvements. First, our model considers nitrogen as the only limiting nutrient, even though silicate could be another important nutrient (Townsend *et al.*, 2006). Given the distinct silicate sources between coastal and offshore regions, silicate dynamics might potentially regulate phytoplankton community heterogeneity, especially during spring blooms when diatoms are dominant over the entire shelf. Phosphate is not usually treated as the limiting nutrient in the NAS, while recent field measurements suggest its importance in summer (Townsend *et al.*, 2014). Future modelling development needs to carefully assess the role of other potentially limiting nutrients.

Global eco-evolutionary model results suggest the thermal adaptation can mitigate the loss of phytoplankton diversity owing to its rapid reproduction (Thomas *et al.*, 2012). However, designing a parameterization scheme to well represent phytoplankton adaptation to rapid warming is still challenging due to the lack of thermal adaptation information in a variety of taxa. Considering the distinct responses to warming between different phytoplankton species (Staeher and Birkeland, 2006), characterizing thermal adaptation of the dominant species in the NAS system becomes essential in climate projection of future ecosystem responses.

Many field measurements and laboratory cultures indicate phytoplankton sinking velocity varies dramatically, and it is influenced by many factors such as nutrient availability, morphological features of cells, and physical environments (Bienfang *et al.*, 1983). Besides, some species of large diatoms undergo bursts of rapid sinking (sinking velocity increases from almost zero to 0.2 mm s^{-1} in several seconds), and such behavior benefits the growth of diatom by enhancing nutrient flux to cell surface (Gemmell *et al.*, 2016). All these findings suggest the constant sinking velocity scheme employed in most biological models might not be able to adequately resolve phytoplankton vertical settling flux, and such an oversimplification can introduce substantial uncertainties in simulating primary production, carbon sequestration, and benthic–pelagic coupling (Griffiths *et al.*, 2017). In future studies, a dynamic phytoplankton sinking velocity scheme should be developed and applied to biological models to better represent phytoplankton settling process.

Conclusions

A 3D physical–biogeochemical model was applied in the NAS ecosystem to investigate the seasonality of phytoplankton dynamics and the underlying mechanisms modulating its spatial heterogeneity. The spatial heterogeneity on the NAS resulted from the joint influences of nutrient availability and temperature-related physiology: a strong impact of nutrient limitation in the MAB lead to an earlier winter bloom and a later fall bloom, while a delayed spring bloom and an advanced fall bloom in the GoM could be attributed to the dominance of temperature limiting effect. Chlorophyll concentrations at the surface and bottom were coupled, whereas stratification and mixing, interaction with slope water, and resuspension attributed to the decoupling between bottom detritus and surface productivity. Given the importance of phytoplankton in the marine food web, its spatial heterogeneity over the NAS could impact trophic connections between phytoplankton and zooplankton. The differences in thermohaline structure and warming mecha-

nisms between the GoM and the MAB contributed to the distinct responses of phytoplankton abundance to climate-related warming in the two regions. Most biogeochemical models could only partially reproduce the impact of warming on the marine ecosystem due to their simplified structures. To better simulate the impact of rapid warming on phytoplankton dynamics on the NAS, parameterizations of numerous temperature-related processes (e.g. stratification, nutrient cycling, and zooplankton grazing) should be improved in the future.

Supplementary data

Supplementary material is available at the ICESJMS online version of the manuscript.

Data availability

The original marine food web model data underlying this article will be shared on a reasonable request to the corresponding author. The processed bimonthly MARMAP phytoplankton size structure data with 0.5° resolution in our study region is available at http://ulyse2.who.edu:8080/thredds/catalog/data/zzang/MARMAP_bimonth/catalog.html.

Acknowledgements

This study was supported by NOAA Coastal and Ocean Climate Application (COCA) Program (NA17OAR4310273) and NSF Northeast US Shelf–Long-Term Ecological Research (NES-LTER) Program (OCE-1655686). Computational support was provided by HPC system (cluster Poseidon) at WHOI. The model results and processed observation data are stored in WHOI HPC system. Kimberly Hyde and Chris Melrose provided the original MARMAP size-fractionated phytoplankton data. This study greatly benefited from discussions with the NES-LTER team members and Yun Li at University of Delaware. Constructive comments and suggestions from two anonymous reviewers and editor are much appreciated.

References

- Ariathurai, R., and Arulanandan, K. 1978. Erosion rates of cohesive soils. *Journal of the Hydraulics Division*, 104: 279–283.
- Arin, L., Marrasé, C., Maar, M., Peters, F., Sala, M. - M., and Alcaraz, M. 2002. Combined effects of nutrients and small-scale turbulence in a microcosm experiment. I. Dynamics and size distribution of osmotrophic plankton. *Aquatic Microbial Ecology*, 29: 51–61.
- Balch, W., Huntington, T., Aiken, G., Drapeau, D., Bowler, B., Lubelczyk, L., and Butler, K. 2016. Toward a quantitative and empirical dissolved organic carbon budget for the Gulf of Maine, a semi-enclosed shelf sea. *Global Biogeochemical Cycles*, 30: 268–292.
- Belkin, I. M. 2009. Rapid warming of large marine ecosystems. *Progress in Oceanography*, 81: 207–213.
- Bienfang, P. K., Szyper, J., and Laws, E. 1983. Sinking rate and pigment responses to light-limitation of a marine diatom—implications to dynamics of chlorophyll maximum layers. *Oceanologica Acta*, 6: 55–62.
- Burrows, M. T., Schoeman, D. S., Buckley, L. B., Moore, P., Poloczanska, E. S., Brander, K. M., Brown, C. *et al.* 2011. The pace of shifting climate in marine and terrestrial ecosystems. *Science*, 334: 652–655.
- Butman, B., Aretxabaleta, A. L., Dickhudt, P. J., Dalyander, P. S., Sherwood, C. R., Anderson, D. M., Keafer, B. A. *et al.* 2014. Investigating the importance of sediment resuspension in *Alexandrium fundyense* cyst population dynamics in the Gulf of Maine. *Deep Sea Research Part II: Topical Studies in Oceanography*, 103: 79–95.
- Chen, C., Huang, H., Beardsley, R. C., Xu, Q., Limeburner, R., Cowles, G. W., Sun, Y. *et al.* 2011. Tidal dynamics in the Gulf of Maine and New England Shelf: an application of FVCOM. *Journal of Geophysical Research*, 116: C12010. <https://doi.org/10.1029/2011JC007054>.
- Chen, C., Liu, H., and Beardsley, R. C. 2003. An unstructured grid, finite-volume, three-dimensional, primitive equations ocean model: application to coastal ocean and estuaries. *Journal of Atmospheric and Oceanic Technology*, 20: 159–186.
- Chen, C., Malanotte-Rizzoli, P., Wei, J., Beardsley, R. C., Lai, Z., Xue, P., Lyu, S. *et al.* 2009. Application and comparison of Kalman filters for coastal ocean problems: an experiment with FVCOM. *Journal of Geophysical Research*, 114: C05011. <https://doi.org/10.1029/2007JC004548>.
- Chen, K., Gawarkiewicz, G. G., Lentz, S. J., and Bane, J. M. 2014. Diagnosing the warming of the Northeastern U.S. Coastal Ocean in 2012: a linkage between the atmospheric jet stream variability and ocean response. *Journal of Geophysical Research: Oceans*, 119: 218–227.
- Cranford, P. J., and Gordon, D. C. 1992. The influence of dilute clay suspensions on sea scallop (*Placopecten magellanicus*) feeding activity and tissue growth. *Netherlands Journal of Sea Research*, 30: 107–120.
- Damashek, J., and Francis, C. A. 2018. Microbial nitrogen cycling in estuaries: from genes to ecosystem processes. *Estuaries and Coasts*, 41: 626–660.
- Dunne, J. P., Armstrong, R. A., Gnanadesikan, A., and Sarmiento, J. L. 2005. Empirical and mechanistic models for the particle export ratio. *Global Biogeochemical Cycles*, 19, GB4026: GB4026.
- Eppley, R. W. 1972. Temperature and phytoplankton growth in the sea. *Fish Bull*, 70: 1063–1085.
- Fennel, K., Wilkin, J., Levin, J., Moisan, J., O'Reilly, J., and Haidvogel, D. 2006. Nitrogen cycling in the Middle Atlantic Bight: results from a three-dimensional model and implications for the North Atlantic nitrogen budget. *Global Biogeochemical Cycles*, 20: GB3007. <https://doi.org/10.1029/2005GB002456>.
- Fennel, K., Wilkin, J., Previdi, M., and Najjar, R. 2008. Denitrification effects on air-sea CO₂ flux in the coastal ocean: simulations for the Northwest North Atlantic. *Geophysical Research Letters*, 35: L24608. <https://doi.org/10.1029/2008GL036147>.
- Friedrichs, M. A. M., St-Laurent, P., Xiao, Y., Hofmann, E., Hyde, K., Mannino, A., Najjar, R. G. *et al.* 2019. Ocean circulation causes strong variability in the Mid-Atlantic Bight Nitrogen Budget. *Journal of Geophysical Research: Oceans*, 124: 113–134.
- Geider, R. J., MacIntyre, H. L., and Kana, T. M. 1997. Dynamic model of phytoplankton growth and acclimation: responses of the balanced growth rate and the chlorophyll a:carbon ratio to light, nutrient-limitation and temperature. *Marine Ecology Progress Series*, 148: 187–200.
- Gemmell, B. J., Oh, G., Buskey, E. J., and Villareal, T. A. 2016. Dynamic sinking behaviour in marine phytoplankton: rapid changes in buoyancy may aid in nutrient uptake. *Proceedings of the Royal Society B: Biological Sciences*, 283: 20161126. <https://doi.org/10.1098/rspb.2016.1126>.
- Gentleman, W., Leising, A., Frost, B., Strom, S., and Murray, J. 2003. Functional responses for zooplankton feeding on multiple resources: a review of assumptions and biological dynamics. *Deep Sea Research Part II: Topical Studies in Oceanography*, 50: 2847–2875.
- Goode, A. G., Brady, D. C., Steneck, R. S., and Wahle, R. A. 2019. The brighter side of climate change: how local oceanography amplified a lobster boom in the Gulf of Maine. *Global Change Biology*, 25: 3906–3917.
- Griffiths, J. R., Kadin, M., Nascimento, F. J. A., Tamelander, T., Törnroos, A., Bonaglia, S., Bonsdorff, E. *et al.* 2017. The importance of benthic–pelagic coupling for marine ecosystem functioning in a changing world. *Global Change Biology*, 23: 2179–2196.
- Hu, S., Chen, C., Ji, R., Townsend, D. W., Tian, R., Beardsley, R. C., and Davis, C. S. 2011. Effects of surface forcing on interannual variability of the fall phytoplankton bloom in the gulf of maine revealed using a process-oriented model. *Marine Ecology Progress Series*, 427: 29–49.

- Hu, S., Townsend, D. W., Chen, C., Cowles, G., Beardsley, R. C., Ji, R., and Houghton, R. W. 2008. Tidal pumping and nutrient fluxes on Georges Bank: a process-oriented modeling study. *Journal of Marine Systems*, 74: 528–544.
- Hyde, K. J. W., O'Reilly, J. E., and Oviatt, C. A. 2007. Validation of SeaWiFS chlorophyll a in Massachusetts Bay. *Continental Shelf Research*, 27: 1677–1691.
- Ji, R., Davis, C., Chen, C., and Beardsley, R. 2008a. Influence of local and external processes on the annual nitrogen cycle and primary productivity on Georges Bank: a 3D biological-physical modeling study. *Journal of Marine Systems*, 73: 31–47.
- Ji, R., Davis, C. S., Chen, C., Townsend, D. W., Mountain, D. G., and Beardsley, R. C. 2008b. Modeling the influence of low-salinity water inflow on winter-spring phytoplankton dynamics in the Nova Scotian Shelf–Gulf of Maine region. *Journal of Plankton Research*, 30: 1399–1416.
- Ji, R., Davis, C. S., Chen, C., Townsend, D. W., Mountain, D. G., and Beardsley, R. C. 2007. Influence of ocean freshening on shelf phytoplankton dynamics. *Geophysical Research Letters*, 34: L24607. <https://doi.org/10.1029/2007GL032010>.
- Laurent, A., Fennel, K., Wilson, R., Lehrter, J., and Devereux, R. 2016. Parameterization of biogeochemical sediment-water fluxes using *in situ* measurements and a diagenetic model. *Biogeosciences*, 13: 77–94.
- Li, W. K. W., Glen Harrison, W., and Head, E. J. H. 2006. Coherent assembly of phytoplankton communities in diverse temperate ocean ecosystems. *Proc R Soc*, 273: 1953–1960.
- Li, Y., Fratantoni, P. S., Chen, C., Hare, J. A., Sun, Y., Beardsley, R. C., and Ji, R. 2015. Spatio-temporal patterns of stratification on the Northwest Atlantic shelf. *Progress in Oceanography*, 134: 123–137.
- Loder, J. W. 1998. The coastal ocean off northeastern North America: a large-scale view. *In* *The Sea*, 11, pp. 105–133. Ed. by Robinson, A. R., and Brink, K. H., John Wiley, New York, NY.
- Loder, J. W., Van Der Baaren, A., and Yashayaev, I. 2015. Climate comparisons and change projections for the Northwest Atlantic from Six CMIP5 models. *Atmosphere-Ocean*, 53: 529–555.
- Malone, T. C., Hopkins, T. S., Falkowski, P. G., and Whitley, T. E. 1983. Production and transport of phytoplankton biomass over the continental shelf of the new york bight. *Continental Shelf Research*, 1: 305–337.
- Margalef, R. 1978. Life-forms of phytoplankton as survival alternatives in an unstable environment. *Oceanologica Acta*, 1: 493–509.
- Maritorena, S., d'Andon, O. H. F., Mangin, A., and Siegel, D. A. 2010. Merged satellite ocean color data products using a bio-optical model: characteristics, benefits and issues. *Remote Sensing of Environment*, 114: 1791–1804.
- Miles, T., Seroka, G., Kohut, J., Schofield, O., and Glenn, S. 2015. Glider observations and modeling of sediment transport in Hurricane Sandy. *Journal of Geophysical Research: Oceans*, 120: 1771–1791.
- Mills, K. E., Pershing, A. J., Brown, C. J., Chen, Y., Chiang, F. S., Holland, D. S., Lehuta, S. *et al.* 2013. Fisheries management in a changing climate: lessons from the 2012 ocean heat wave in the Northwest Atlantic. *Oceanography*, 26: 191–195.
- Moriarty, J. M., Harris, C. K., Friedrichs, M. A. M., Fennel, K., and Xu, K. 2018. Impact of seabed resuspension on oxygen and nitrogen dynamics in the northern Gulf of Mexico: a numerical modeling study. *Journal of Geophysical Research: Oceans*, 123: 7237–7263.
- Mountain, D. G., and Manning, J. P. 1994. Seasonal and interannual variability in the properties of the surface waters of the Gulf of Maine. *Continental Shelf Research*, 14: 1555–1581.
- Mouw, C. B., and Yoder, J. A. 2010. Optical determination of phytoplankton size composition from global SeaWiFS imagery. *Journal of Geophysical Research*, 115: C12018. <https://doi.org/10.1029/2010JC006337>.
- Mouw, C. B., and Yoder, J. A. 2005. Primary production calculations in the Mid-Atlantic Bight, including effects of phytoplankton community size structure. *Limnology and Oceanography*, 50: 1232–1243.
- O'Reilly, J. E., and Busch, D. A. 1984. Phytoplankton primary production on the northwestern Atlantic shelf. *Rapp PV Reun Cons Int Explor Mer*, 183: 255–268.
- O'Reilly, J. E., and Zetlin, C. A. 1998. Seasonal, horizontal, and vertical distribution of phytoplankton chlorophyll a in the northeast US continental shelf ecosystem, NOAA Technical Report NMFS 139, U.S. Dep. of Commer., Seattle.
- Pan, X., Mannino, A., Marshall, H. G., Filippino, K. C., and Mulholland, M. R. 2011. Remote sensing of phytoplankton community composition along the northeast coast of the United States. *Remote Sensing of Environment*, 115: 3731–3747.
- Pershing, A. J., Alexander, M. A., Hernandez, C. M., Kerr, L. A., Le Bris, A., Mills, K. E., Nye, J. A. *et al.* 2015. Slow adaptation in the face of rapid warming leads to collapse of the Gulf of Maine cod fishery. *Science*, 350: 809–812.
- Pershing, A. J., and Stamieszkin, K. 2020. The North Atlantic Ecosystem, from Plankton to Whales. *Annual Review of Marine Science*, 12: 339–359.
- Ramp, S. R., Schlitz, R. J., and Wright, W. R. 1985. The deep flow through the Northeast Channel, Gulf of Maine. *Journal of Physical Oceanography*, 15: 1790–1808.
- Rebeck, N. D., and Townsend, D. W. 2014. A climatology and time series for dissolved nitrate in the Gulf of Maine region. *Deep Sea Research Part II: Topical Studies in Oceanography*, 103: 223–237.
- Ross, O. N. 2006. Particles in motion: how turbulence affects plankton sedimentation from an oceanic mixed layer. *Geophysical Research Letters*, 33: L10609. <https://doi.org/10.1029/2006GL026352>.
- Ryan, J. P., Yoder, J. A., and Cornillon, P. C. 1999. Enhanced chlorophyll at the shelfbreak of the Mid-Atlantic Bight and Georges Bank during the spring transition. *Limnology and Oceanography*, 44: 1–11.
- Schoudele, A. 1996. The seasonal variation of nutrients in three Maine estuaries. M.Sc. Thesis, University of New Hampshire, Durham, NH. 103.
- Shearman, R. K., and Lentz, S. J. 2010. Long-term sea surface temperature variability along the US East Coast. *Journal of Physical Oceanography*, 40: 1004–1017.
- Sherman, E., Moore, J. K., Primeau, F., and Tanouye, D. 2016. Temperature influence on phytoplankton community growth rates. *Global Biogeochemical Cycles*, 30: 550–559. <https://doi.org/10.1002/2015GB005272>. Received.
- Song, H., Ji, R., Stock, C., Kearney, K., and Wang, Z. 2011. Interannual variability in phytoplankton blooms and plankton productivity over the Nova Scotian Shelf and in the Gulf of Maine. *Marine Ecology Progress Series*, 426: 105–118.
- Song, H., Ji, R., Stock, C., and Wang, Z. 2010. Phenology of phytoplankton blooms in the Nova Scotian Shelf-Gulf of Maine region: remote sensing and modeling analysis. *Journal of Plankton Research*, 32: 1485–1499.
- Staehr, P. A., and Birkeland, M. J. 2006. Temperature acclimation of growth, photosynthesis and respiration in two mesophilic phytoplankton species. *Phycologia*, 45: 648–656.
- Staudinger, M. D., Mills, K. E., Stamieszkin, K., Record, N. R., Hudak, C. A., Allyn, A., Diamond, A. *et al.* 2019. It's about time: a synthesis of changing phenology in the Gulf of Maine ecosystem. *Fisheries Oceanography*, 28: 532–566.
- Stock, C. A., and Dunne, J. 2010. Controls on the ratio of mesozooplankton production to primary production in marine ecosystems. *Deep Sea Research Part I: Oceanographic Research Papers*, 57: 95–112.
- Stock, C. A., Powell, T. M., and Levin, S. A. 2008. Bottom-up and top-down forcing in a simple size-structured plankton dynamics model. *Journal of Marine Systems*, 74: 134–152.
- Sun, Y., Chen, C., Beardsley, R. C., Ullman, D., Butman, B., and Lin, H. 2016. Surface circulation in Block Island Sound and adjacent coastal and shelf regions: a FVCOM-CODAR comparison. *Progress in Oceanography*, 143: 26–45.
- Sun, Y., Chen, C., Beardsley, R. C., Xu, Q., Qi, J., and Lin, H. 2013. Impact of current-wave interaction on storm surge simulation: a case study for Hurricane Bob. *Journal of Geophysical Research: Oceans*, 118: 2685–2701.

- Switzer, M., Townsend, D., and Pettigrew, N. 2020. The effects of source water masses and internal recycling on concentrations of dissolved inorganic nutrients in the Gulf of Maine. *Continental Shelf Research*, 204: 104157. <https://doi.org/10.1016/j.csr.2020.104157>.
- Thomas, A. C., Pershing, A. J., Friedland, K. D., Nye, J. A., Mills, K. E., Alexander, M. A., Record, N. R. *et al.* 2017. Seasonal trends and phenology shifts in sea surface temperature on the North American northeastern continental shelf. *Elementa: Science of the Anthropocene*, 5: 48. <https://doi.org/10.1525/elementa.240>.
- Thomas, A. C., Townsend, D. W., and Weatherbee, R. 2003. Satellite-measured phytoplankton variability in the Gulf of Maine. *Continental Shelf Research*, 23: 971–989.
- Thomas, M. K., Kremer, C. T., Klausmeier, C. A., and Litchman, E. 2012. A global pattern of thermal adaptation in marine phytoplankton. *Science*, 338: 1085–1088.
- Tian, R., Chen, C., Qi, J., Ji, R., Beardsley, R. C., and Davis, C. 2014. Model study of nutrient and phytoplankton dynamics in the Gulf of Maine: patterns and drivers for seasonal and interannual variability. *ICES Journal of Marine Science*, 72: 388–402.
- Townsend, D. W. 1998. Sources and cycling of nitrogen in the Gulf of Maine. *Journal of Marine Systems*, 16: 283–295.
- Townsend, D. W., and Cammen, L. M. 1988. Potential importance of the timing of spring plankton blooms to benthic-pelagic coupling and recruitment of juvenile demersal fishes. *Biol Oceanogr*, 5: 215–228.
- Townsend, D. W., McGillicuddy, D. J., Thomas, M. A., and Rebeck, N. D. 2014. Nutrients and water masses in the Gulf of Maine-Georges Bank region: variability and importance to blooms of the toxic dinoflagellate *Alexandrium fundyense*. *Deep Sea Research Part II: Topical Studies in Oceanography*, 103: 238–263.
- Townsend, D. W., Rebeck, N. D., Thomas, M. A., Karp-Boss, L., and Gettings, R. M. 2010. A changing nutrient regime in the Gulf of Maine. *Continental Shelf Research*, 30: 820–832.
- Townsend, D. W., Thomas, A. C., Mayer, L. M., Thomas, M. A., and Quinlan, J. A. 2006. Oceanography of the northwest Atlantic continental shelf. *In* *The Sea*, 14, pp. 119–168. Ed. by Robinson, A. R., and Brink, K. H.. Harvard University Press, Cambridge MA.
- Van Oostende, N., Dussin, R., Stock, C. A., Barton, A. D., Curchitser, E., Dunne, J. P., and Ward, B. B. 2018. Simulating the ocean's chlorophyll dynamic range from coastal upwelling to oligotrophy. *Progress in Oceanography*, 168: 232–247.
- Xu, Y., Chant, R., Gong, D., Castelao, R., Glenn, S., and Schofield, O. 2011. Seasonal variability of chlorophyll a in the Mid-Atlantic Bight. *Continental Shelf Research*, 31: 1640–1650.
- Yoder, J. A., O'Reilly, J. E., Barnard, A. H., Moore, T. S., and Ruhsam, C. M. 2001. Variability in coastal zone color scanner (CZCS) Chlorophyll imagery of ocean margin waters off the US East Coast. *Continental Shelf Research*, 21: 1191–1218.
- Yoder, J. A., Schollaert, S. E., and O'Reilly, J. E. 2002. Climatological phytoplankton chlorophyll and sea surface temperature patterns in continental shelf and slope waters off the northeast US coast. *Limnology and Oceanography*, 47: 672–682.
- Zhang, S., Stock, C. A., Curchitser, E. N., and Dussin, R. 2019. A numerical model analysis of the mean and seasonal nitrogen budget on the Northeast US Shelf. *Journal of Geophysical Research: Oceans*, 124: 2969–2991.
- Zhang, W. G., McGillicuddy, D. J., and Gawarkiewicz, G. G. 2013. Is biological productivity enhanced at the New England shelfbreak front? *Journal of Geophysical Research: Oceans*, 118: 517–535.

Handling editor: Matt Oliver